PCCP

PAPER

View Article Online
View Journal | View Issue

Check for updates

Cite this: *Phys. Chem. Chem. Phys.*, 2021, **23**, 10059

Nonlinear light absorption in many-electron systems excited by an instantaneous electric field: a non-perturbative approach†

Alberto Guandalini,[ab] Caterina Cocchi,[cd] Stefano Pittalis,[a] Alice Ruini[b] and Carlo Andrea Rozzi*[a]

Received 18th September 2020,
Accepted 13th April 2021

DOI: 10.1039/d0cp04958a

rsc.li/pccp

Applications of low-cost non-perturbative approaches in real time, such as time-dependent density functional theory, for the study of nonlinear optical properties of large and complex systems are gaining increasing popularity. However, their assessment still requires the analysis and understanding of elementary dynamical processes in simple model systems. Motivated by the aim of simulating optical nonlinearities in molecules, here exemplified by the case of the quaterthiophene oligomer, we investigate light absorption in many-electron interacting systems beyond the linear regime by using a single broadband impulse of an electric field; *i.e.* an electrical impulse in the instantaneous limit. We determine non-pertubatively the absorption cross section from the Fourier transform of the time-dependent induced dipole moment, which can be obtained from the time evolution of the wavefunction. We discuss the dependence of the resulting cross section on the magnitude of the impulse and we highlight the advantages of this method in comparison with perturbation theory by working on a one-dimensional model system for which numerically exact solutions are accessible. Thus, we demonstrate that the considered non-pertubative approach provides us with an effective tool for investigating fluence-dependent nonlinear optical excitations.

Open Access Article. Published on 14 April 2021. Downloaded on 6/14/2026 5:53:56 AM.
This article is licensed under a Creative Commons Attribution-NonCommercial 3.0 Unported Licence.

1 Introduction

Nonlinear optics globally refers to the regime in which the polarization induced in a material by an electric field is not directly proportional to the magnitude of the external field. All optical media are intrinsically nonlinear, but it is only with the development of high power lasers that nonlinear properties have become experimentally accessible and, hence, extensively studied.[1–3]

The standard theoretical approach to nonlinear optics rests on perturbation theory, in which the polarization induced in a quantum system by a (classical) electric field is expressed as a power series in the field strength.[4] Susceptibilities calculated at the first few finite orders are usually of interest. Second- and higher-order response function theory has been derived in different flavors and levels of accuracy.[5–28] In this way, nonlinear phenomena such as second harmonic generation,[29] optical rectification,[30–32] and multi-photon absorption in molecular systems[33,34] can be described.

The development of femtosecond and attosecond lasers has pushed the largest available peak intensity toward magnitudes of the electric field comparable with (or larger than) those experienced by electrons in the atoms.[35] These light sources have thus provided direct access to a variety of resonant regimes in which perturbation theory is not suitable either because the perturbation series does not converge or because its use is impractical.[36] To explore the corresponding phenomenology, a non-perturbative solution is in order.[37–39]

Direct numerical time-propagation of a quantum state subject to time-dependent fields provides us with a numerical approach that, in principle, does not suffer from the limitation of perturbative series expansions.[40,41] In fact, nonlinear properties both at finite order in the perturbation[42–44] and at all orders[45–49] can be obtained. First-principles approaches such as time-dependent density functional theory (TDDFT)[50,51] enable realistic simulations of both steady-state and time-resolved spectroscopies for large systems that cannot be tackled by means of more accurate but also more computationally

[a] *CNR - Istituto Nanoscienze, Via Campi 213A, I-41125 Modena, Italy. E-mail: carloandrea.rozzi@nano.cnr.it*
[b] *Dipartimento di Scienze Fisiche, Informatiche e Matematiche, Università di Modena e Reggio Emilia, Via Campi 213A, I-41125 Modena, Italy*
[c] *Physics Department and IRIS Adlershof, Humboldt-Universität zu Berlin, Zum Großen Windkanal 2, D-12489 Berlin, Germany*
[d] *Physics Department, Carl von Ossietzky Universität Oldenburg, Carl-von-Ossietzky-Straße 9, 26129 Oldenburg, Germany*

† Electronic supplementary information (ESI) available. See DOI: 10.1039/d0cp04958a

Open Access Article. Published on 14 April 2021. Downloaded on 6/14/2026 5:53:56 AM.
This article is licensed under a Creative Commons Attribution-NonCommercial 3.0 Unported Licence.

demanding methods.[46,52–54] The linear and nonlinear regimes can, in principle, be tackled on equal footings within the same framework.[55] Moreover, the inclusion of nuclear dynamics is straightforward.[56–63] Extensions for describing the propagation in presence of decoherence, dissipative environments, or coupling to other external degrees of freedom are also available.[64]

When applied to compute the linear-response of a system, the time-propagation method is often formulated in terms of impulse response theory in order to extract the *entire* frequency window of interest by means of a single impulse – given that the time propagation can be run long enough. For time-invariant dynamical systems, the impulse response to an external perturbation is a property of the unperturbed system and is independent of the specific temporal shape of the perturbation: Given the knowledge of the impulse response alone, it is possible to predict the response to any small perturbation by means of the convolution theorem.[65] In the linear regime, this procedure is equivalent to calculating the first-order polarizability.[66]

Although the aforementioned procedure breaks down as the nonlinear effects become important, it can be extended to compute the nonlinear frequency-dependent cross section in such a way that the determination of the density-density response function does not enter explicitly any step. As we demonstrate below, the procedure is appealing particularly because it can work well when a perturbative approach is challenged by a slow (or a lack of) convergence. The methodology we consider was proposed and applied within the framework of real-time TDDFT in the work by Cocchi *et al.*[55] to study optical power limiting due to reverse saturable absorption (RSA) in organic molecules.

RSA is the property of materials to increase their light-absorption efficiency at increasing intensity of the incoming field, due to the presence of an available channel for excited state absorption.[67,68] It can be described either through phenomenological models[69] or in the framework of perturbation theory through a two-step procedure. First, the initial excited state has to be computed and then, from it, the optical absorption spectrum has to be determined.[70–79] However, these methods are limited to one (or at most a few) absorption channels given *a priori*, which hinders the generality of the results. In contrast, the real-time methodology by Cocchi *et al.*[55] can capture RSA without any assumption about the excitation channels. The kind of the nonlinear process that drives the RSA may justify the success of the aforementioned approach: As long as the steady-state absorption is observed by means of continuous wave lasers (*i.e.*, we are only concerned with a time-invariant observable) the spectrum depends on the intensity, but not on the detailed shape or phase of the impinging light.

However, for these processes, the interpretation of the results based on TDDFT rests so far on empirical grounds, due to the difficulty of disentangling the approximations introduced by TDDFT from the information provided by the impulsive response. In particular, the adiabatic approximation – common to essentially all the state-of-the-art TDDFT calculations – is difficult to improve systematically.[80–84] Moreover, it is well known that the errors implied by the specific approximations for the ground-state exchange–correlations functional (invoked within in the adiabatic approximation) can vary largely from one form to another.[85] The dependence of the results on these approximations can be expected to be stronger when dealing with nonlinear excitations and, thus, further systematic evaluations would be required. Last but not least, it may also be necessary to access interacting quantities which are not directly available in TDDFT, which provides only the time-dependent particle density.

Here, we elaborate on some of the open questions by analyzing the nonlinear absorption spectrum of quaterthiophene oligomer (4T) computed *via* the nonpertubative TDDFT technique as introduced in ref. 55 (all the relevant details on the procedure are provided below). To gain non-empirical insights into these results and of the likes, we also study the response to instantaneous non-perturbative probes of a model system for which numerically exact solutions are accessible. This will grant us valuable information to control real-time TDDFT simulations in the same regime and thus to exploit their full potential.

This work is organized as follows: In Section 2, we present and analyze the linear and nonlinear absorption spectra of 4T, highlighting the current shortcomings in the interpretation of these results. In Section 3 the expression of the absorption cross section and its spectral resolution is analytically derived for an instantaneous impulsive exciting field of arbitrary strength within the dipole approximation. The cross section is analyzed both in the nonlinear case and in the weak-field limit. The complementarity between the proposed non-perturbative methodology and regular perturbative theory is discussed. In Section 4 the linear and nonlinear absorption of two electrons interacting in a 1D infinite well is simulated by means of an accurate numerical time-propagation scheme. The absorption cross section of the model system is interpreted, determining the contribution of ground-state and excited-state absorption at different field strengths. Finally, the validity, the usefulness, and limitations of the proposed non-perturbative methodology to simulate nonlinear properties in complex materials are discussed.

2 Nonlinear optical absorption of quaterthiophene

We start our study by applying the non-perturbative approach introduced in ref. 55 to access the nonlinear optical response of 4T, a popular oligomer in the research field of organic semiconductors.[86] While often adopted to model segments of polymeric chains,[87–89] this molecule absorbs visible radiation,[90–93] which makes it technologically relevant *per se* upon suitable functionalization.[94–97]

Before moving on to the analysis of the results, we briefly comment on the computational costs. In ref. 98, the computational details of the devised procedure are reported, where linear and

 This journal is © the Owner Societies 2021

Open Access Article. Published on 14 April 2021. Downloaded on 6/14/2026 5:53:56 AM.
This article is licensed under a Creative Commons Attribution-NonCommercial 3.0 Unported Licence.

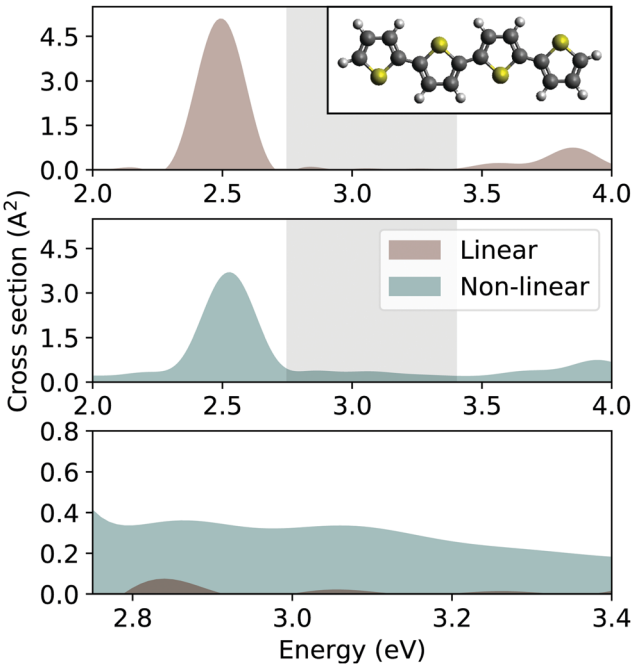

Fig. 1 Absorption cross section of the 4T oligomer computed from real-time TDDFT using the non-linear impulse approach from ref. 55 in the linear regime (top panel) and in the nonlinear one (middle panel). The grey shaded area marks the optical limiting region for which the linear and nonlinear cross sections are overlaid on the bottom panel. Inset: 4T molecule in the ball-and-stick representation, with C atoms in grey, S atoms in yellow, and H atoms in white.

nonlinear regime are accessible on the same footing and with comparable numerical efforts. It should be noticed, though, that the access to nonlinear properties requires a proper adjustment of the basis set or, like in the present case, of the simulation box size, in order to prevent numerical artifacts.

The linear absorption cross section of 4T as computed from real-time TDDFT[98] (see Fig. 1, top panel) exhibits the first, intense peak centered at about 2.5 eV, in agreement with previous experimental[90–93,99] and theoretical results.[100–103] At higher energies, above 3.5 eV, a weaker absorption band appears, again, in agreement with previous TDDFT predictions.[103] Between these two regions of absorption, the spectrum is characterized by a transparent window, which is highlighted in Fig. 1. Inspecting now the cross section computed in the nonlinear regime (see Fig. 1, middle panel), we notice that the aforementioned region is no longer transparent (see Fig. 1, bottom panel). This increase of absorption in that window occurs at the expenses of the first peak, which looses oscillator strength compared to the linear regime. This is a typical signature of RSA, the main driving mechanism of optical limiting.[3,55,104] Additional calculations of the same type could be performed at varying values of the impulsive perturbation to probe the intensity-dependence of the nonlinear response, as performed in ref. 55. This would correspondingly impact on the computational costs.

The results presented in Fig. 1 demonstrate the general applicability of the non-linear impulse approach in the framework of real-time TDDFT, to calculate the nonlinear optical absorption of molecules and atomic cluster, and predict intriguing properties such as optical limiting. However, from these results, we cannot say much about the origin of this behavior, and a number of open questions remain. For example: (i) Why do the peaks in linear absorption spectrum loose oscillator strength and what determines the corresponding amount?; (ii) What is the fundamental physical origin behind the increasing absorption in the transparent window in linear regime? (iii) Is it possible to relate the optical response obtained in the adopted non-perturbative approach with that given by perturbation theory?

In order to overcome this troublesome lack of understanding, it is necessary to take a step back and apply the proposed non-perturbative approach to systems that we are able to tackle *via* accurate *ab initio* methodology or to restrict ourselves to model systems that can be solved exactly. In this way, we can look at the behavior of interacting quantities which are not directly accessible *via* TDDFT (which directly provides us the time-dependent particle density only). Moreover, we can focus on the output of the methodology – *i.e.*, probing the systems *via* instantaneous, intense electrical fields – disentangled from the effects of an approximation of TDDFT or other numerical intricacies which may be met for complex systems. In return, the gained insight obtained with this strategy can provide valuable information to consciously and effectively embed this method in real-time TDDFT simulations, in order to exploit its full potential.

3 Absorption cross section in the instantaneous impulsive limit

Let us consider a system of N interacting electrons subject to a time-dependent classical electric field in the dipole approximation, described by the Hamiltonian $\hat{H}(t) = \hat{H}_0 - \hat{d}_\mu \mathscr{E}_\mu(t)$ (summation over repeated indices is understood), where $\hat{H}_0$ includes the ordinary electron–nuclei and electron–electron Coulomb interaction, $\hat{d}_\mu = \sum_{i=1}^{N} \hat{r}^i_\mu$ is the electric dipole operator with $\hat{r}^i_\mu$, and $\mu = x,y,z$ is the μ-th component of the position operator of the i-th electron. Spin–orbit coupling is neglected. We aim to describe the light absorption process in the case of an extremely short pulse, *i.e.* in the limit of a Dirac-delta time-dependence

$$\mathscr{E}_\mu(t) = \kappa_\mu \delta(t). \quad (1)$$

The quantity κ_μ is a constant specifying direction and magnitude of the instantaneous electric field.[66] In the dipole approximation it is independent of the spatial coordinates. We make no particular assumption about the value of $\kappa \equiv \sqrt{\kappa_\mu \kappa_\mu}$. Here, we focus our analysis on absorption at equilibrium, *i.e.*, we suppose that the system is in its ground state at $t < 0$, namely $|\Psi(t < 0)\rangle = |\Psi_0\rangle e^{-iE_0 t}$. For a description of the out-of-equilibrium absorption processes, as in the case of time-resolved absorption spectroscopy, further analysis is required.[105]

Open Access Article. Published on 14 April 2021. Downloaded on 6/14/2026 5:53:56 AM.
This article is licensed under a Creative Commons Attribution-NonCommercial 3.0 Unported Licence.

For $t > 0$, the solution of the time-dependent Schrödinger equation $|\Psi(t)\rangle$ can be projected onto the eigenstates $\{|\Psi_i\rangle\}$ of $\hat{H}_0$ as

$$|\Psi(t>0)\rangle = \sum_{i=0}^{+\infty} c_i |\Psi_i\rangle e^{-iE_i t}, \tag{2}$$

where $\{E_i\}$ are the eigenvalues of $\hat{H}_0$. The coefficients c_i are

$$c_i = \langle \Psi_i | e^{-i\hat{d}_\mu \kappa_\mu} | \Psi_0 \rangle. \tag{3}$$

Due to the instantaneous nature of the perturbation, the c_i coefficients are time-independent. The time-dependent dipole moment $d_\mu(t) = \langle \Psi(t)|\hat{d}_\mu|\Psi(t)\rangle$ for such a system is

$$d_\mu(t) = \theta(t) \sum_{i,j=0}^{+\infty} c_i^* c_j d_\mu^{ij} e^{-i\omega_{ji}t} + \theta(-t) d_\mu^{00}, \tag{4}$$

where $\theta(t)$ is the Heaviside theta function, $d_\mu^{ij} = \langle \Psi_i|\hat{d}_\mu|\Psi_j\rangle$ are the dipole matrix elements, d_μ^{00} is the ground state dipole, and $\omega_{ji} = E_j - E_i$ is the energy difference between the j-th and i-th eigenstates of the unperturbed Hamiltonian $\hat{H}_0$.

We now want to employ the explicit shape for the dipole moment in eqn (4) in order to calculate the absorption cross section

$$\sigma(\omega) = \frac{4\pi\omega}{c} \frac{\mathrm{Im}\left[d_\mu(\omega)\mathcal{E}_\mu^*(\omega)\right]}{|\mathcal{E}(\omega)|^2}. \tag{5}$$

The full derivation of eqn (5) is provided in the ESI,† showing that this expression is not limited to the weak-field regime. The way we will make use of eqn (5) deserves an important clarification: we will report below absorption spectra computed beyond the linear regime which therefore will be referred to as non-linear spectra. This terminology is used for simplicity and it is not meant to hint that such non-linear spectra can be measured experimentally by employing a single band-limited laser.

By Fourier transforming eqn (4), substituting it into eqn (5), and assuming, for sake of simplicity, that the system is centrosymmetric (*i.e.*, $d_\mu^{00} = 0$), we obtain

$$\sigma(\omega) = \frac{4\pi^2}{c\kappa^2} \sum_{i,j>i} \left[C_{0i}S_{j0} - S_{0i}C_{j0}\right] M_{ij}\omega_{ji}\delta(\omega_{ji} - \omega), \tag{6}$$

where $C_{ij} \equiv \langle \Psi_i|\cos(\hat{d}_\mu\kappa_\mu)|\Psi_j\rangle$, $S_{ij} \equiv \langle \Psi_i|\sin(\hat{d}_\mu\kappa_\mu)|\Psi_j\rangle$, and $M_{ij}^{(n)} \equiv \langle \Psi_i|(\hat{d}_\mu\kappa_\mu)^n|\Psi_j\rangle$, with $M_{ij}^{(1)} \equiv M_{ij}$. Eqn (6), derived in the ESI,† can be used to describe any centrosymmetric system, or an ensemble of non-centrosymmetric objects randomly oriented with respect to the direction of the electric field. Since the ensemble-averaged optical response is centrosymmetric regardless of the point symmetry of the individual molecules, the average cross section is obtained by sampling and averaging the responses to impulses with different polarization directions.

In order to highlight the nonlinear character of the cross section, we compute the linear absorption cross section $\sigma^{(1)}(\omega)$ by approximating the matrix elements in eqn (6) up to the first order in κ. We can physically define the concept of "small κ" since the magnitude of the dipole is limited by the spatial extension R of the system. For molecular systems with $R \approx (1-100)$ Bohr, $\hat{d}_\mu\kappa_\mu \ll 1$ when $\kappa \ll 1/R$. Therefore, $\kappa \approx 10^{-3}$ Bohr^{-1} is suitable to define a weak field in the impulsive limit.[66] Since $\sin(\hat{d}_\mu\kappa_\mu) \approx \hat{d}_\mu\kappa_\mu$ and $\cos(\hat{d}_\mu\kappa_\mu) \approx \hat{1}$, we have

$$\sigma^{(1)}(\omega) = \frac{4\pi^2\omega}{c\kappa^2} \sum_{j=0}^{+\infty} |M_{j0}|^2 \delta(\omega - \omega_{j0}). \tag{7}$$

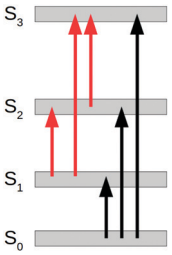

Fig. 2 Sketch of ground-state (black) and excited-state (red) excitations in the singlet manifold. Excited-state excitations involve transitions between excited states and are activated in the nonlinear regime described by eqn (6). Ground-state absorption is described by the ordinary linear cross section in eqn (7).

For small κ (in the above-mentioned sense), eqn (7) provides a good approximation for eqn (6).

While in the linear regime the resonances in the cross section are only found at $\omega = \omega_{j0} \equiv E_j - E_0$, in eqn (6) the resonances occur at $\omega = \omega_{ji} \equiv E_j - E_i$; *i.e.*, for the energy of the incoming light equating the energy difference between any pair of eigenstates of the unperturbed Hamiltonian $\hat{H}_0$. This is sketched in Fig. 2, in which black arrows indicate ground-state absorption (GSA), as given by eqn (7), and red arrows denote excited-state absorption (ESA), as given by eqn (6). ESA, in practice, can occur when one or more excited states of the unperturbed system are populated by a laser.

Eqn (6) and (7) share the same dipole parity selection rule, as they include the same matrix elements M_{ij}, with $i = 0$ in eqn (7). However, while states with the same parity as the ground state cannot be populated in the linear regime, they can be populated in the nonlinear regime through ESA. Further, the individual contributions to eqn (6) vanish for all the states i with either $C_{0i} = 0$, or $S_{0i} = 0$. In the next section, we exploit this fact to determine the set of transitions that build up the ESA at different field strengths. Also note that in eqn (6) $\sigma(\omega)$ satisfies the Thomas–Reiche–Kuhn sum rule in the form

$$\int_0^{+\infty} d\omega \sigma(\omega) = \frac{2\pi^2 N}{c}, \tag{8}$$

where N is the number of electrons. Since the right hand side of eqn (8) does not depend on κ, the sum rule is valid both in the linear and nonlinear regimes.

The perturbative analysis can be carried on by further expanding eqn (6) in powers of κ. The second-order term, like all subsequent terms of even order, vanishes because we assumed inversion symmetry. The third-order term is

$$\sigma^{(3)}(\omega) = \frac{4\pi^2}{c\kappa^2}\left[\sigma_{\mathrm{GSA}}^{(3)}(\omega) + \sigma_{\mathrm{ESA}}^{(3)}(\omega)\right], \tag{9}$$

 This journal is © the Owner Societies 2021

Open Access Article. Published on 14 April 2021. Downloaded on 6/14/2026 5:53:56 AM.
This article is licensed under a Creative Commons Attribution-NonCommercial 3.0 Unported Licence.

where

$$\sigma^{(3)}_{\mathrm{GSA}}(\omega) \equiv -\frac{1}{6}\sum_j \left(M_{0j} M^{(3)}_{j0} + 3 M^{(2)}_{00} |M_{j0}|^2 \right) \omega_{j0} \delta(\omega - \omega_{j0}) \tag{10}$$

has poles only at the ground state excitation energies $\omega_{j0} = E_j - E_0$ (see eqn (7)): *i.e.*, it describes the third-order correction to GSA. Hence, the term

$$\sigma^{(3)}_{\mathrm{ESA}}(\omega) \equiv -\frac{1}{2}\sum_{\substack{i>0 \\ j>i}} \left(M^{(2)}_{0i} M_{j0} - M_{0i} M^{(2)}_{j0} \right) M_{ij} \omega_{ji} \delta(\omega - \omega_{ji}) \tag{11}$$

describes the third-order correction to ESA. Note that $\sigma^{(3)}$ includes both excitations and de-excitations from the excited states. The spectral features obtained from the nonlinear cross section may therefore have either positive or negative oscillator strengths, physically corresponding to light absorption or emission from an excited state. Next, the fifth-order correction is derived in a similar way as done for the third-order one:

$$\begin{aligned} \sigma^{(5)}(\omega) \; = & \frac{4\pi^2 \omega}{c\kappa^2} \Bigg\{ \frac{1}{120} \sum_j M^{(5)}_{j0} M_{0j} \omega_{j0} \delta(\omega - \omega_{j0}) \\ & + \frac{1}{12} \sum_{i,j>i} \left[M^{(2)}_{0i} M^{(3)}_{j0} - M^{(3)}_{0i} M^{(2)}_{j0} \right] M_{ij} \omega_{ji} \delta(\omega - \omega_{ji}) \\ & + \frac{1}{24} \sum_{i,j>i} \left[M^{(4)}_{0i} M_{j0} - M_{0i} M^{(4)}_{j0} \right] M_{ij} \omega_{ji} \delta(\omega - \omega_{ji}) \Bigg\}. \end{aligned} \tag{12}$$

GSA and ESA contributions can be identified for $\sigma^{(5)}$ similarly as done for $\sigma^{(3)}$, by isolating the terms with $i = 0$ in the latter expression (see Section S3 in the ESI†). We will make use of Eqn (7), (9) and (12) in the next section.

Even if eqn (9) also accounts for two-photon processes, the impulsive field has a fixed frequency dependence. Therefore, it cannot predict spectra obtained by means of non-impulsive field shapes. On the other hand, eqn (9) allows us to directly identify the spectral weight due to specific set of transitions at a common resonance. Consequently, accessing $\sigma(\omega)$ with an instantaneous impulse is most useful to describe ESA (which is fluence dependent) but it is not suitable for a full description of two-photon absorption (which is irradiance dependent).[106]

Obviously, the impulse response obtained from real-time propagation of the quantum state is intrinsically non perturbative: namely, from the evolved quantum state we compute $d_\mu(t) = \langle \Psi(t) | \hat{d}_\mu | \Psi(t) \rangle$ and, thus, the Fourier transform $d_\mu(\omega)$ can be readily obtained. The latter can be finally used in eqn (5). According to the previous analysis, the approach captures ESA at *all* the possible resonances. Furthermore, because $d_\mu(t)$ can be expressed in terms of the particle density, $d_\mu(t) = \int d^3 r r_\mu n(\mathbf{r}, t)$, the procedure based on real-time propagation can be readily implemented in any code that solves the time-dependent Kohn–Sham equations without the need for the explicit knowledge of the many-body wave function. Thus, large systems can be tackled efficiently within TDDFT approximations.[55]

Before moving to the next section – where the numerical application to a model system and the related careful analytical investigation allow to gain further insights – we emphasize that spin–orbit coupling and magnetic fields are not included in our considerations. We work under the assumption that the ground state is a spin singlet, thus, both expressions in eqn (6) and eqn (7) allow transitions only within the manifold of *singlet* excited states. Studying the absorption of excited states with different spin multiplicity is important, for example, to account for inter-system crossing[107] which can occur in optical limiting processes. Formally, this would require to use spin-dependent impulses.[108,109]

4 Analysis of nonlinear absorption in a 1D model system

Here, we scrutinize the information that can be retrieved by the ''real-time impulsive method'' on the cross section of an interacting system beyond the linear regime. Our choice to work at the level of a simple model system, instead of a real molecule, allows us to avoid from the outset the challenge of the typical approximations of state-of-the-art TDDFT. Below, we also compare results from the perturbative expressions derived in the previous section with the computed non-perturbative solution obtained by directly time-evolving the many-body sate.

The considered system consists of two interacting electrons confined in a one-dimensional segment by a potential well of infinite depth (hereafter 1DW). The unperturbed Hamiltonian of the 1DW is

$$\hat{H}_0 = \sum_{i=1}^{2} \left[-\frac{1}{2} \frac{\partial^2}{\partial {x_i}^2} + v_{\mathrm{ext}}(x_i) \right] + \frac{1}{\sqrt{1 + (x_1 - x_2)^2}}, \tag{13}$$

with the external potential

$$v_{\mathrm{ext}}(x_i) = \begin{cases} 0 & -L/2 < x_i < L/2 \\ \infty & \text{otherwise} \end{cases}. \tag{14}$$

The second term in eqn (13) is the Coulomb interaction between the two electrons, which is softened to avoid the singularity at $x_1 = x_2$.[110] For the numerical simulation, we have employed the Octopus code.[111,112] $\hat{H}_0$ is symmetric under particle interchange $x_1 \leftrightarrow x_2$. Hence, we can choose the spatial component of the wavefunction to be either symmetric or antisymmetric with respect to the exchange of the spatial coordinates. The eigenstates belong to the irreducible representation of either singlet or triplet spin multiplicity. In addition, $\hat{H}_0$ has also spatial inversion symmetry. Consequently, the orbital part of the wavefunctions must be either even or odd under inversion of the coordinates.

The time-dependent polarization is calculated as $d(t) = \langle \Psi(t) | \hat{d} | \Psi(t) \rangle$ and its Fourier transform $\tilde{d}(\omega)$ enters the absorption cross section

$$\sigma(\omega) = \frac{4\pi\omega}{c} \frac{\mathrm{Im}[\tilde{d}(\omega)]}{\kappa}. \tag{15}$$

The eigenstates and eigenfunctions of this system are shown in Fig. 3. The singlet and triplet states are labeled as S_i and T_i,

Open Access Article. Published on 14 April 2021. Downloaded on 6/14/2026 5:53:56 AM.
This article is licensed under a Creative Commons Attribution-NonCommercial 3.0 Unported Licence.

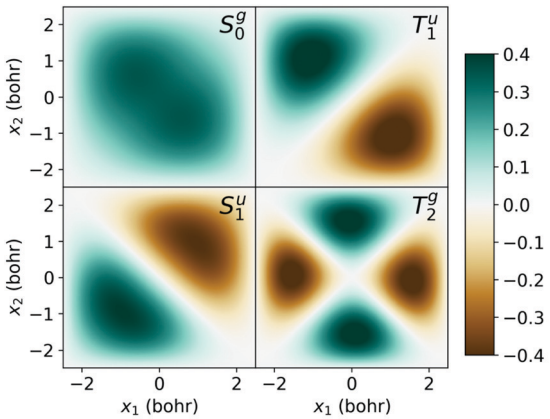

State	Energy (Ha)	State	Energy (Ha)
S_0^g	1.09		
S_1^u	1.76	T_1^u	1.47
S_2^g	2.17	T_2^g	2.53
S_3^g	2.72	T_3^u	3.05
S_4^u	3.26	T_4^u	3.95
S_5^u	4.05	T_5^g	4.49

Fig. 3 Plot: Eigenstates depicted in the configuration space x_1–x_2 (left) of the unperturbed system of two electrons in a 1D potential well of infinite depth (eqn (13)). The states are labeled as $S_i^{g/u}$, where S indicates the spin state (singlet S or triplet T), i the order in energy within the spin channel, and g/u the parity with respect to inversion of the coordinates. Colorbar units are Bohr^{-1}. Table: Eigenvalues of the first five eigenvectors of the unperturbed Hamiltonian in eqn (13).

respectively, where the subscript i labels the ground state ($i = 0$) as well as the excited states ($i > 0$). The superscripts g (gerade) and u (ungerade) indicate the parity of the wavefunction. Due to the parity selection rules, dipole transitions are only allowed between g and u states. In addition, the spin selection rule $\Delta S = 0$ holds, as the perturbed Hamiltonian is spin-independent. Thus, the only allowed transitions are $S_i^g \rightarrow S_j^u$ and $S_i^u \rightarrow S_j^g$ in both the linear and nonlinear regimes.

The linear and nonlinear absorption spectra of the 1DW obtained by applying an electric field impulse with $\kappa = 0.01$ Bohr^{-1} and 0.80 Bohr^{-1}, respectively, are shown in Fig. 4. Given the well length and the spacing of the ground-state eigenvalues, the field corresponding to $\kappa \leq 0.02$ Bohr^{-1} can be considered weak. The resulting cross sections show an intrinsic broadening of 0.04 Ha due to the finite duration of the time propagation.

In the upper panel of Fig. 4 the linear spectrum shows a single maximum at 0.67 Ha, corresponding to the $S_0^g \rightarrow S_1^u$ transition. In contrast, the nonlinear absorption cross section features several peaks spread over the range (0.4–1.4) Ha, namely at lower and higher energies with respect to the excitation in the linear regime. In the nonlinear regime, the maximum corresponding to the $S_0^g \rightarrow S_1^u$ transition at 0.67 Ha is not suppressed but its spectral weight is approximately halved.

To analyze the transitions involved in the nonlinear cross section, in Fig. 5 we consider separately the contributions of three components, namely $\sigma_{S_0}(\omega)$, $\sigma_{S_1}(\omega)$, and $\sigma_{\{S_m\}}(\omega)$, with $m \geq 2$. The first and second components account for the absorption from

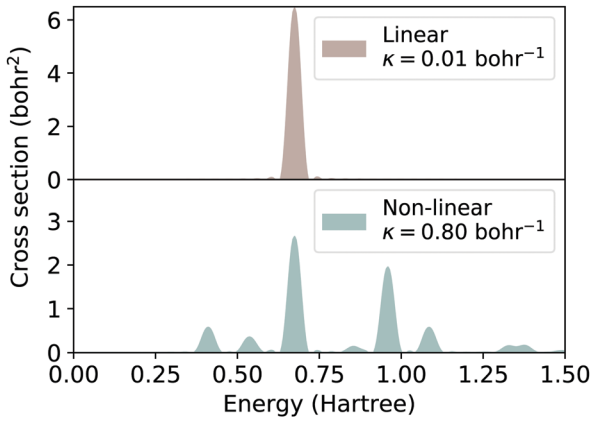

Fig. 4 Comparison between the linear and nonlinear absorption spectra of a 1D square potential well containing two electrons (1DW). The linear absorption spectrum (upper panel) is obtained by applying an impulsive electric field with strength κ = 0.01 Bohr^{-1} (weak-field regime). The nonlinear absorption spectrum (lower panel) is obtained by applying an electric field with strength κ = 0.80 Bohr^{-1} (strong field regime).

the ground state and from the first excited state, while the third one includes the contributions from all higher excited states. These components are calculated from eqn (6) evaluating the sums up to the first 100 eigenstates of $\hat{H}_0$. Convergence is ensured by the sum rule in eqn (8). Dirac deltas in eqn (6) are broadened in order to match the peak width of the cross sections obtained from the solution of the time-dependent Schrödinger equation.

The component $\sigma_{S_0}(\omega)$ (top panel of Fig. 5) includes the same contribution as the linear cross section, $S_0^g \rightarrow S_1^u$ (see top panel of Fig. 4). Therefore, the additional peaks in the lower panel of Fig. 4 result from ESA. In particular, the two peaks at 0.41 Ha and 0.96 Ha (see middle panel of Fig. 5) are due to the absorption from the first excited state (S_1^u) and involve the transitions to gerade excited states $S_1^u \rightarrow S_2^g$ and $S_1^u \rightarrow S_3^g$,

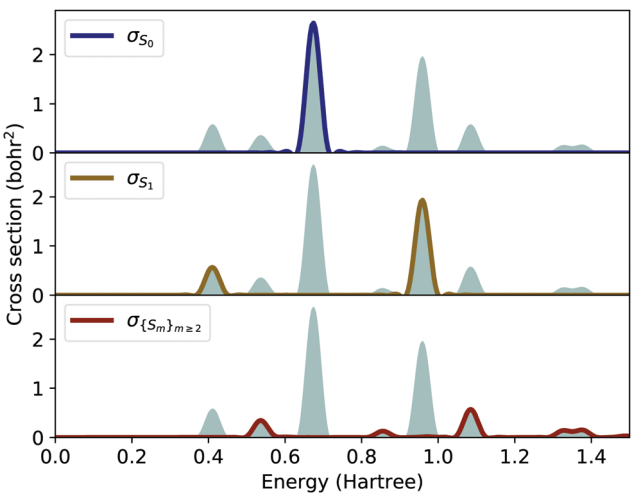

Fig. 5 Nonlinear absorption cross section of the 1DW subject to a strong electric field impulse with κ = 0.80 Bohr^{-1}. The cross section is split into ground-state absorption (blue curve), first excited-state absorption (yellow curve) and absorption from higher excited states (red curve).

This journal is © the Owner Societies 2021

Open Access Article. Published on 14 April 2021. Downloaded on 6/14/2026 5:53:56 AM.
This article is licensed under a Creative Commons Attribution-NonCommercial 3.0 Unported Licence.

respectively. Simply based on symmetry, the excited states S_2^g and S_3^g cannot be reached from the ground state S_0^g. By inspecting the bottom panel of Fig. 5, we notice that the higher-order contributions to the absorption consist of a number of weak peaks below and above the maximum at 0.67 Ha. For example, the maximum at about 1.1 Ha corresponds to the transition $S_2^g \rightarrow S_4^u$.

To gain further understanding on the information provided by the non-perturbative approach presented so far, it is interesting to inspect the variation of the relative weights of GSA and ESA as a function of the field strength. These contributions are quantified by

$$I_{S_i} = \frac{c}{4\pi^2}\int_0^{+\infty} d\omega \sigma_{S_i}(\omega). \quad (16)$$

The values of I_{S_0}, I_{S_1}, and I_{S_m}, with $m \geq 2$, are shown in Fig. 6 as a function of κ. Note that each contribution refers to a specific subset of the absorption but they all include contributions *at all perturbation orders*. The solid curve in Fig. 6 represents the weight of the ground-state cross section I_{S_0}. For $\kappa \approx 0$, we have that $I_{S_0} \approx 1$, which confirms that there is only GSA in the linear regime, as expected. At increasing values of κ, I_{S_0} decreases monotonically: ESA becomes relevant as the response of the system deviates from linearity. For $\kappa > 1.44$ Bohr^{-1}, we have that $I_{S_0} < 0.05$, meaning that GSA becomes negligible above this threshold. The dashed curve in Fig. 6 represents the weight of the first-excited-state cross section I_{S_1}. It vanishes for small κ, reaches its maximum at $\kappa = 0.85$ Ha, and decreases monotonically for higher values of κ. The dashed-dotted curve in Fig. 6 accounts for the weight of the higher-order absorption cross section $I_{\{S_m\}}$, where $m \geq 2$. Also $I_{\{S_m\}}$ does not contribute at small κ. It increases monotonically starting from $\kappa \approx 0.25$ Bohr^{-1} and reaches its saturation value, $I_{\{S_m\}} = 1$, for κ approaching 2 Bohr^{-1}. In the strong field limit ($\kappa > 1.75$ Bohr^{-1}), the only non-negligible component of the cross section is $I_{\{S_m\}}$.

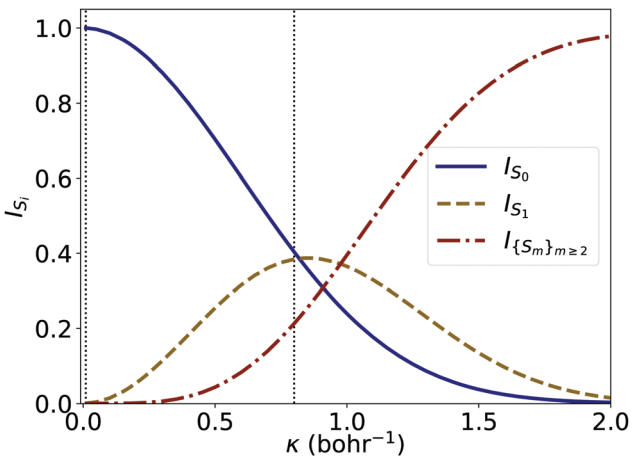

Fig. 6 Normalized weights [see eqn (16)] of the three components of the absorption cross section given in Fig. 5 as a function of the strength of the electric field impulse κ. The dashed vertical bars correspond to the values of κ used in Fig. 4.

We complete our analysis by considering the perturbative expansion of the nonlinear absorption cross section, as discussed in Section 3. The perturbative terms $\sigma^{(1)}(\omega)$, $\sigma^{(3)}(\omega)$, and $\sigma^{(5)}(\omega)$ are shown in on the left panel of Fig. 7. They are computed from eqn (7), (9) and (12). The cross section $\sigma(\omega)$ calculated with the impulse response method for $\kappa = 0.80$ Bohr^{-1} is also shown for reference. For comparison, on the right panel of Fig. 7 we show the perturbative contribution summed up to the indicated order.

The first-order cross section $\sigma^{(1)}(\omega)$ assumes only positive values and contributes only to the maximum at 0.67 Ha. The first nonlinear non-vanishing component of the cross section, which thus accounts for ESA processes, is the third-order one, $\sigma^{(3)}$, which assumes both positive and negative values. A pronounced peak with negative strength is found at 0.67 Ha and corresponds to the third-order correction of the ground-state transition $S_0^g \rightarrow S_1^u$. This term cancels out almost completely the contribution from $\sigma^{(1)}$ at the same energy. Maxima with positive intensities appear at about 0.4 Ha and 1.0 Ha.

However, the contribution of $\sigma^{(3)}$ alone is not sufficient to describe the nonlinear excitations in the 1DW – see Fig. 7, left panel, middle graph. For this purpose, it is necessary to include at least also the contributions from the fifth-order cross section, $\sigma^{(5)}$. This term has maxima and minima at the same energy as those of $\sigma^{(3)}$ but with intensities of opposite sign. In particular, the peak at 0.67 Ha is positive and overlaps almost perfectly with the one in the impulse cross section shown in the background. Minima are found at approximately 0.4 Ha and 1.0 Ha, at the same energies where $\sigma^{(3)}$ exhibits maxima. The absolute values of the corresponding intensities are very similar, suggesting that these contributions should cancel out. We stress the fact that summing up the perturbative contributions of σ up to the fifth order is still not sufficient to match the non-perturbative result. Even assuming that the perturbative series is within its convergence radius (which is not trivially granted), Fig. 7 shows that for large values of κ the terms of the series tend to have alternating sign contributions, which explains the observed difficulties in the convergence.

5 Discussion

Before moving to our general conclusions, we look back at the linear and nonlinear absorption spectra computed for the 4T molecule (see Fig. 1). Although the spectral region considered in that case was significantly narrower in energy than the one examined in the 1DW model (see Fig. 4), we can recognize some common features. First and foremost, with the exactly solvable system, we have clarified that the oscillator strength arising above the absorption onset in the linear regime stems from excited-state absorption that can be associated to specific contributions in the perturbative expansion of the total cross section (see Fig. 7). Also the loss of spectral weight of the first peak in the nonlinear regime is explained as a renormalization due to the high-order contributions to the cross section. Finally, nonlinear effects

Open Access Article. Published on 14 April 2021. Downloaded on 6/14/2026 5:53:56 AM.
This article is licensed under a Creative Commons Attribution-NonCommercial 3.0 Unported Licence.

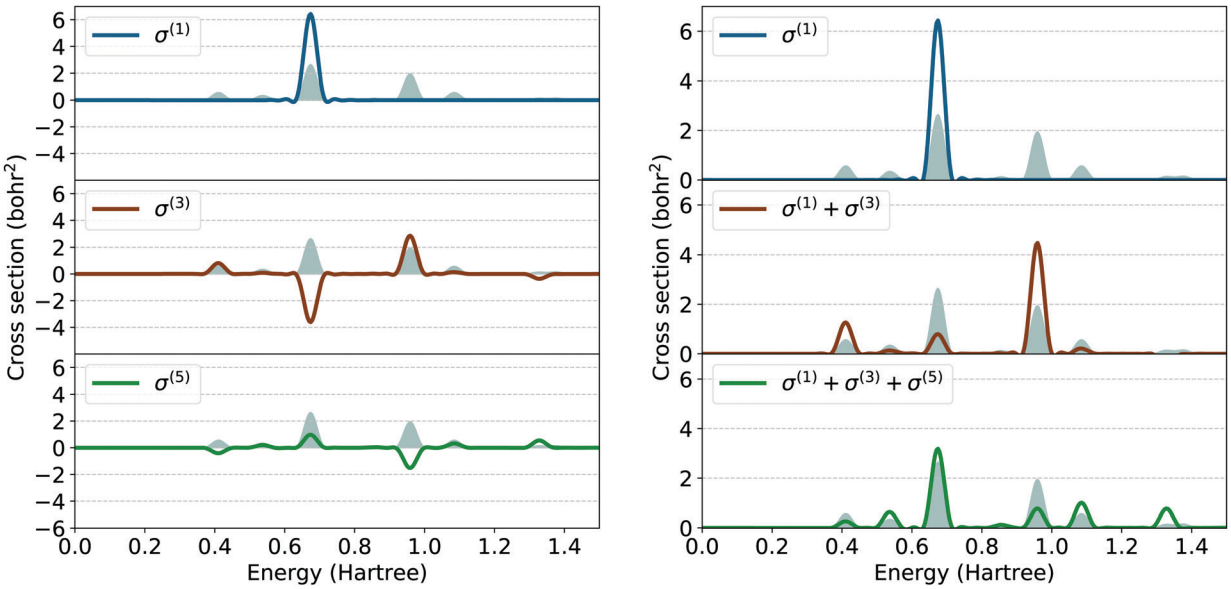

Fig. 7 Left panel: Perturbative components $\sigma^{(1)}$, $\sigma^{(3)}$ and $\sigma^{(5)}$ (Eqn (7), (9) and (12) respectively) of the nonlinear absorption cross section the 1DW subject to the electric field impulse $\kappa = 0.80$ Bohr^{-1}. For reference, the total cross section (eqn (6)), also shown in the bottom panel of Fig. 4, is plotted as shaded area in the background of each panel. Right panel: Summation of the first five non-zero terms in the perturbation series compared to the full non-perturbative result (shaded grey area).

are responsible for the enhanced absorption below the linear absorption onset.

We stress that the impulse approach cannot access the dependence of the spectrum on the pulse shape. Therefore, it cannot be exploited, as it is, to study processes such as two-photon absorption or ultrafast transients. It is not suitable either to investigate those cases in which hysteresis loops or other memory-dependent phenomena are important. However, for cases in which the interest in optical nonlinearities is not restricted to wave mixing at a predefined order, or at a single frequency, the computation of observables from real-time propagation in the nonlinear impulsive excitation regime is particularly useful to perform a wide-band quick check for the presence of non-linear effects outperforming the ordinary approach based on perturbation theory. In fact this technique does not make use of unoccupied states, which implies a number of computational advantages: it is not affected by the convergence issues of perturbative methods or by the choice of an active space; it is equally stable on and off-resonance (at difference, for example, with Sternheimer's method[28]); its sensitivity is controlled by the same parameters as a linear propagation (namely, time step and total propagation time); it is easily scalable; it is easily integrated with a nuclear dynamics scheme.

These features render this method an ideal tool to scan materials for potential interesting non-linearities induced by excited state absorption such as reverse saturable absorption, optical switching, and optical limiting.

6 Conclusions and outlook

In conclusion, we have shown that the time-evolution of many-electron systems induced by an electric field in the instantaneous limit is an effective tool for investigating computationally fluence-dependent nonlinear optical properties. It works well also for those cases in which the convergence of the perturbative expansions of the cross sections is challenging. Specifically, we have shown that the impulsive method provides relevant information about the steady-state absorption of time-invariant systems in which the nonlinear effects manifest themselves merely as a function of the field fluence.

One of the main advantages of the impulse technique is that the nonlinear absorption cross section is promptly obtained at computational costs that are comparable with those needed for linear response in real time and certainly much lower with respect to conventional perturbative approaches. This method is deliberately designed to take advantage of an infinite bandwidth excitation to search for optical nonlinearities of a system. Its application in the framework of real-time TDDFT to a free-base phthalocyanine molecule demonstrated that the outcome of optical limiting experiments based on the Z-scan technique[113] can be successfully reproduced.[55]

We envision additional theoretical work in the near future that systematically analyzes the impact of approximations of TDDFT also beyond the linear regime. We are confident that these developments will provide the community with novel, powerful computational tools that are able to complement emerging experimental directions in ultrafast spectroscopy.[114–116]

Conflicts of interest

There are no conflicts to declare.

This journal is © the Owner Societies 2021

Open Access Article. Published on 14 April 2021. Downloaded on 6/14/2026 5:53:56 AM.
This article is licensed under a Creative Commons Attribution-NonCommercial 3.0 Unported Licence.

Acknowledgements

A. G. acknowledges financial support from the German Academic Exchange Service (DAAD) grant n. 57440917 and from HPC Europa 3 grant no HPC17AS2HO. C. C. appreciates funding from the German Research Foundation (DFG), Project number 182087777 – SFB 951, from the German Federal Ministry of Education and Research (Professorinnenprogramm III) as well as from the State of Lower Saxony (Professorinnen für Niedersachsen). Computational resources provided by the North-German Supercomputing Alliance (HLRN), project bep00060, and by the High Performance Computing Center Stuttgart (HLRS). S. P. acknowledges financial support through MIUR PRIN Grant No. 2017RKWTMY. C. A. R. acknowledges support from MIUR PRIN Grant No. 201795SBA3.

References

1 P. A. Franken, A. E. Hill, C. W. Peters and G. Weinreich, *Phys. Rev. Lett.*, 1961, **7**, 118–119.
2 T. Damm, M. Kaschke, F. Noack and B. Wilhelmi, *Opt. Lett.*, 1985, **10**, 176–178.
3 M. D. Perry and G. Mourou, *Science*, 1994, **264**, 917–924.
4 R. W. Boyd, *Nonlinear Optics, Third Edition*, Academic Press, Inc., USA, 3rd edn, 2008.
5 S. Tretiak and V. Chernyak, *J. Chem. Phys.*, 2003, **119**, 8809–8823.
6 B. I. Grimberg, V. V. Lozovoy, M. Dantus and S. Mukamel, *J. Phys. Chem. A*, 2002, **106**, 697–718.
7 I. Tunell, Z. Rinkevicius, O. Vahtras, P. Sałek, T. Helgaker and H. Ågren, *J. Chem. Phys.*, 2003, **119**, 11024–11034.
8 B. Jansik, P. Sałek, D. Jonsson, O. Vahtras and H. Ågren, *J. Chem. Phys.*, 2005, **122**, 054107.
9 S. J. A. van Gisbergen, J. G. Snijders and E. J. Baerends, *J. Chem. Phys.*, 1998, **109**, 10644–10656.
10 M. de Wergifosse and S. Grimme, *J. Chem. Phys.*, 2018, **149**, 024108.
11 H. Hait Heinze, F. Della Sala and A. Görling, *J. Chem. Phys.*, 2002, **116**, 9624–9640.
12 J. Henriksson, T. Saue and P. Norman, *J. Chem. Phys.*, 2008, **128**, 024105.
13 G. Senatore and K. R. Subbaswamy, *Phys. Rev. A: At., Mol., Opt. Phys.*, 1987, **35**, 2440–2447.
14 J.-I. Iwata, K. Yabana and G. F. Bertsch, *J. Chem. Phys.*, 2001, **115**, 8773–8783.
15 A. Ye and J. Autschbach, *J. Chem. Phys.*, 2006, **125**, 234101.
16 D. R. Kanis, M. A. Ratner and T. J. Marks, *J. Am. Chem. Soc.*, 1992, **114**, 10338–10357.
17 O. Quinet, B. Champagne and B. Kirtman, *J. Comput. Chem.*, 2001, **22**, 1920–1932.
18 O. Quinet and B. Champagne, *Int. J. Quantum Chem.*, 2001, **85**, 463–468.
19 O. Quinet and B. Champagne, *J. Chem. Phys.*, 2002, **117**, 2481–2488.
20 D. Jonsson, P. Norman and H. Ågren, *J. Chem. Phys.*, 1996, **105**, 6401–6419.
21 O. Berman and S. Mukamel, *Phys. Rev. A: At., Mol., Opt. Phys.*, 2003, **67**, 042503.
22 H. Hettema, H. J. A. Jensen, P. Jo/rgensen and J. Olsen, *J. Chem. Phys.*, 1992, **97**, 1174–1190.
23 A. Ye, S. Patchkovskii and J. Autschbach, *J. Chem. Phys.*, 2007, **127**, 074104.
24 P. Sałek, O. Vahtras, T. Helgaker and H. Ågren, *J. Chem. Phys.*, 2002, **117**, 9630–9645.
25 Z. Rinkevicius, P. C. Jha, C. I. Oprea, O. Vahtras and H. Ågren, *J. Chem. Phys.*, 2007, **127**, 114101.
26 P. Elliott, S. Goldson, C. Canahui and N. T. Maitra, *Chem. Phys.*, 2011, **391**, 110–119.
27 S. M. Parker, D. Rappoport and F. Furche, *J. Chem. Theory Comput.*, 2018, **14**, 807–819.
28 X. Andrade, S. Botti, M. A. L. Marques and A. Rubio, *J. Chem. Phys.*, 2007, **126**, 184106.
29 E. Luppi, H. Hübener and V. Véniard, *Phys. Rev. B: Condens. Matter Mater. Phys.*, 2010, **82**, 235201.
30 J. L. P. Hughes and J. E. Sipe, *Phys. Rev. B: Condens. Matter Mater. Phys.*, 1996, **53**, 10751–10763.
31 M. Veithen, X. Gonze and P. Ghosez, *Phys. Rev. B: Condens. Matter Mater. Phys.*, 2005, **71**, 125107.
32 L. Prussel and V. Véniard, *Phys. Rev. B*, 2018, **97**, 205201.
33 D. H. Friese, M. T. P. Beerepoot, M. Ringholm and K. Ruud, *J. Chem. Theory Comput.*, 2015, **11**, 1129–1144.
34 D. H. Friese, R. Bast and K. Ruud, *ACS Photonics*, 2015, **2**, 572–577.
35 T. Brabec and F. Krausz, *Rev. Mod. Phys.*, 2000, **72**, 545–591.
36 E. Lorin, M. Lytova, A. Memarian and A. D. Bandrauk, *J. Phys. A: Math. Theor.*, 2015, **48**, 105201.
37 R. L. Peterson, *Rev. Mod. Phys.*, 1967, **39**, 69–77.
38 I. Safi and P. Joyez, *Phys. Rev. B: Condens. Matter Mater. Phys.*, 2011, **84**, 205129.
39 V. V. Strelkov, *Phys. Rev. A*, 2016, **93**, 053812.
40 J. J. Goings, P. J. Lestrange and X. Li, *Wiley Interdiscip. Rev.: Comput. Mol. Sci.*, 2018, **8**, 1–19.
41 M. R. Provorse and C. M. Isborn, *Int. J. Quantum Chem.*, 2016, **116**, 739–749.
42 D. Cho, J. R. Rouxel, M. Kowalewski, P. Saurabh, J. Y. Lee and S. Mukamel, *J. Phys. Chem. Lett.*, 2018, **9**, 1072–1078.
43 F. Ding, B. E. Van Kuiken, B. E. Eichinger and X. Li, *J. Chem. Phys.*, 2013, **138**, 064104.
44 J. Mattiat and S. Luber, *J. Chem. Phys.*, 2018, **149**, 174108.
45 E. Penka Fowe and A. D. Bandrauk, *Phys. Rev. A: At., Mol., Opt. Phys.*, 2011, **84**, 035402.
46 E. Luppi and M. Head-Gordon, *Mol. Phys.*, 2012, **110**, 909–923.
47 T. S. Nguyen, J. H. Koh, S. Lefelhocz and J. Parkhill, *J. Phys. Chem. Lett.*, 2016, **7**, 1590–1595.
48 N. Tancogne-Dejean, O. D. Mücke, F. X. Kärtner and A. Rubio, *Phys. Rev. Lett.*, 2017, **118**, 087403.
49 S. A. Sato, K. Yabana, Y. Shinohara, T. Otobe, K.-M. Lee and G. F. Bertsch, *Phys. Rev. B: Condens. Matter Mater. Phys.*, 2015, **92**, 205413.
50 C. A. Ullrich, *Time-dependent density-functional theory: concepts and applications*, Oxford University Press, Oxford, 2011.

Open Access Article. Published on 14 April 2021. Downloaded on 6/14/2026 5:53:56 AM.
This article is licensed under a Creative Commons Attribution-NonCommercial 3.0 Unported Licence.

51 M. A. Marques, N. T. Maitra, F. M. Nogueira, E. K. U. Gross and A. Rubio, *Fundamentals of Time-Dependent Density Functional Theory*, Springer, Berlin, Heidelberg, 2012.
52 Y. Takimoto, F. D. Vila and J. J. Rehr, *J. Chem. Phys.*, 2007, **127**, 154114.
53 C. Attaccalite and M. Grüning, *Phys. Rev. B: Condens. Matter Mater. Phys.*, 2013, **88**, 1–10.
54 M. Uemoto, Y. Kuwabara, S. A. Sato and K. Yabana, *J. Chem. Phys.*, 2019, **150**, 094101.
55 C. Cocchi, D. Prezzi, A. Ruini, E. Molinari and C. A. Rozzi, *Phys. Rev. Lett.*, 2014, **112**, 1–5.
56 J. L. Alonso, X. Andrade, P. Echenique, F. Falceto, D. Prada-Gracia and A. Rubio, *Phys. Rev. Lett.*, 2008, **101**, 096403.
57 S. M. Falke, C. A. Rozzi, D. Brida, M. Maiuri, M. Amato, E. Sommer, A. De Sio, A. Rubio, G. Cerullo, E. Molinari and C. Lienau, *Science*, 2014, **344**, 1001–1005.
58 S. Pittalis, A. Delgado, J. Robin, L. Freimuth, J. Christoffers, C. Lienau and C. A. Rozzi, *Adv. Funct. Mater.*, 2015, **25**, 2047–2053.
59 C. A. Rozzi, F. Troiani and I. Tavernelli, *J. Phys.: Condens. Matter*, 2017, **30**, 013002.
60 C. A. Rozzi and S. Pittalis, *Handbook of Materials Modeling*, Springer International Publishing, Cham, 2018, pp. 1–19.
61 A. Yamada and K. Yabana, *Phys. Rev. B*, 2019, **99**, 245103.
62 M. Jacobs, J. Krumland, A. M. Valencia, H. Wang, M. Rossi and C. Cocchi, *Adv. Phys.: X*, 2020, **5**, 1749883.
63 J. Krumland, A. M. Valencia, S. Pittalis, C. A. Rozzi and C. Cocchi, *J. Chem. Phys.*, 2020, **153**, 054106.
64 J. Yuen-Zhou, D. G. Tempel, C. A. Rodríguez-Rosario and A. Aspuru-Guzik, *Phys. Rev. Lett.*, 2010, **104**, 043001.
65 R. W. Newcomb, *Proc. IEEE*, 1963, **51**, 1157–1158.
66 K. Yabana and G. F. Bertsch, *Phys. Rev. B: Condens. Matter Mater. Phys.*, 1996, **54**, 4484–4487.
67 D. Dini, M. J. Calvete and M. Hanack, *Chem. Rev.*, 2016, **116**, 13043–13233.
68 Y.-P. Sun and J. E. Riggs, *Int. Rev. Phys. Chem.*, 1999, **18**, 43–90.
69 Q. Miao, Z. Sang, R. Song, M. Liang, Q. Liu, E. Sun and Y. Xu, *J. Photochem. Photobiol., A*, 2019, **385**, 112087.
70 M. de Wergifosse and S. Grimme, *J. Chem. Phys.*, 2019, **150**, 094112.
71 S. A. Fischer, C. J. Cramer and N. Govind, *J. Chem. Theory Comput.*, 2015, **11**, 4294–4303.
72 S. A. Fischer, C. J. Cramer and N. Govind, *J. Phys. Chem. Lett.*, 2016, **7**, 1387–1391.
73 D. N. Bowman, J. C. Asher, S. A. Fischer, C. J. Cramer and N. Govind, *Phys. Chem. Chem. Phys.*, 2017, **19**, 27452–27462.
74 S. Ghosh, J. C. Asher, L. Gagliardi, C. J. Cramer and N. Govind, *J. Chem. Phys.*, 2019, **150**, 104103.
75 P. Elliott and N. T. Maitra, *Phys. Rev. A: At., Mol., Opt. Phys.*, 2012, **85**, 052510.
76 M. A. Mosquera, L. X. Chen, M. A. Ratner and G. C. Schatz, *J. Chem. Phys.*, 2016, **144**, 204105.
77 X. Sheng, H. Zhu, K. Yin, J. Chen, J. Wang, C. Wang, J. Shao and F. Chen, *J. Phys. Chem. C*, 2020, **124**, 4693–4700.
78 Q. Bellier, N. S. Makarov, P.-A. Bouit, S. Rigaut, K. Kamada, P. Feneyrou, G. Berginc, O. Maury, J. W. Perry and C. Andraud, *Phys. Chem. Chem. Phys.*, 2012, **14**, 15299–15307.
79 S. A. Fischer, C. J. Cramer and N. Govind, *J. Phys. Chem. Lett.*, 2016, **7**, 1387–1391.
80 J. I. Fuks and N. T. Maitra, *Phys. Chem. Chem. Phys.*, 2014, **16**, 14504–14513.
81 K. Luo, P. Elliott and N. T. Maitra, *Phys. Rev. A: At., Mol., Opt. Phys.*, 2013, **88**, 042508.
82 J. I. Fuks, P. Elliott, A. Rubio and N. T. Maitra, *J. Phys. Chem. Lett.*, 2013, **4**, 735–739.
83 P. Elliott, J. I. Fuks, A. Rubio and N. T. Maitra, *Phys. Rev. Lett.*, 2012, **109**, 266404.
84 N. T. Maitra, *J. Chem. Phys.*, 2005, **122**, 234104.
85 N. Mardirossian and M. Head-Gordon, *Mol. Phys.*, 2017, **115**, 2315–2372.
86 I. Salzmann, G. Heimel, M. Oehzelt, S. Winkler and N. Koch, *Acc. Chem. Res.*, 2016, **49**, 370–378.
87 L. Zhu, E.-G. Kim, Y. Yi and J.-L. Bredas, *Chem. Mater.*, 2011, **23**, 5149–5159.
88 J. Gao, J. D. Roehling, Y. Li, H. Guo, A. J. Moulé and J. K. Grey, *J. Mater. Chem. C*, 2013, **1**, 5638–5646.
89 M. Arvind, C. E. Tait, M. Guerrini, J. Krumland, A. M. Valencia, C. Cocchi, A. E. Mansour, N. Koch, S. Barlow and S. R. Marder, *et al.*, *J. Phys. Chem. B*, 2020, **124**, 7694–7708.
90 R. Colditz, D. Grebner, M. Helbig and S. Rentsch, *Chem. Phys.*, 1995, **201**, 309–320.
91 D. Grebner, M. Helbig and S. Rentsch, *J. Phys. Chem.*, 1995, **99**, 16991–16998.
92 R. S. Becker, J. Seixas de Melo, A. L. Macanita and F. Elisei, *J. Phys. Chem.*, 1996, **100**, 18683–18695.
93 J. S. de Melo, L. M. Silva, L. G. Arnaut and R. Becker, *J. Chem. Phys.*, 1999, **111**, 5427–5433.
94 G. Barbarella, L. Favaretto, G. Sotgiu, M. Zambianchi, V. Fattori, M. Cocchi, F. Cacialli, G. Gigli and R. Cingolani, *Adv. Mater.*, 1999, **11**, 1375–1379.
95 F. Zhang, D. Wu, Y. Xu and X. Feng, *J. Mater. Chem.*, 2011, **21**, 17590–17600.
96 R. Fitzner, C. Elschner, M. Weil, C. Uhrich, C. Körner, M. Riede, K. Leo, M. Pfeiffer, E. Reinold and E. Mena-Osteritz, *et al.*, *Adv. Mater.*, 2012, **24**, 675–680.
97 H.-W. Lin, W.-Y. Lee, C. Lu, C.-J. Lin, H.-C. Wu, Y.-W. Lin, B. Ahn, Y. Rho, M. Ree and W.-C. Chen, *Polym. Chem.*, 2012, **3**, 767–777.
98 DFT simulations were performed at the Local Density Approximation level within the adiabatic approximation. Kohn–Sham equations (both time-dependent and independent) were solved on a regular spatial grid with a spacing of 0.18 Å on a set of spheres centered at the atomic positions with radius 12 Å. We used an impulse with strength 0.01 and 0.30 $Å^{-1}$ respectively for the linear and non-linear cases. Wavefunctions were propagated up to 20 fs, with a time step of 1.6 as.
99 D. Lap, D. Grebner and S. Rentsch, *J. Phys. Chem. A*, 1997, **101**, 107–112.

 This journal is © the Owner Societies 2021

Open Access Article. Published on 14 April 2021. Downloaded on 6/14/2026 5:53:56 AM.
This article is licensed under a Creative Commons Attribution-NonCommercial 3.0 Unported Licence.

100 D. Beljonne, Z. Shuai and J.-L. Brédas, *J. Chem. Phys.*, 1993, **98**, 8819–8828.
101 G. R. Hutchison, M. A. Ratner and T. J. Marks, *J. Phys. Chem. A*, 2002, **106**, 10596–10605.
102 S. Siegert, F. Vogeler, C. Marian and R. Weinkauf, *Phys. Chem. Chem. Phys.*, 2011, **13**, 10350–10363.
103 C. Cocchi and C. Draxl, *Phys. Rev. B: Condens. Matter Mater. Phys.*, 2015, **92**, 205126.
104 L. W. Tutt and T. F. Boggess, *Prog. Quant. Electron.*, 1993, **17**, 299–338.
105 E. Perfetto and G. Stefanucci, *Phys. Rev. A: At., Mol., Opt. Phys.*, 2015, **91**, 033416.
106 A. Santhi, V. V. Namboodiri, P. Radhakrishnan and V. P. N. Nampoori, *J. Appl. Phys.*, 2006, **100**, 053109.
107 C. M. Marian, *Wiley Interdiscip. Rev.: Comput. Mol. Sci.*, 2012, **2**, 187–203.
108 M. J. T. Oliveira, A. Castro, M. A. L. Marques and A. Rubio, *J. Nanosci. Nanotechnol.*, 2008, **8**, 3392–3398.
109 N. Tancogne-Dejean, F. G. Eich and A. Rubio, *J. Chem. Theory Comput.*, 2020, **16**, 1007–1017.
110 Q. Su and J. H. Eberly, *Phys. Rev. A: At., Mol., Opt. Phys.*, 1991, **44**, 5997–6008.
111 N. Tancogne-Dejean, M. J. T. Oliveira, X. Andrade, H. Appel, C. H. Borca, G. Le Breton, F. Buchholz, A. Castro, S. Corni, A. A. Correa, U. De Giovannini, A. Delgado, F. G. Eich, J. Flick, G. Gil, A. Gomez, N. Helbig, H. Hübener, R. Jestädt, J. Jornet-Somoza, A. H. Larsen, I. V. Lebedeva, M. Lüders, M. A. L. Marques, S. T. Ohlmann, S. Pipolo, M. Rampp, C. A. Rozzi, D. A. Strubbe, S. A. Sato, C. Schäfer, I. Theophilou, A. Welden and A. Rubio, *J. Chem. Phys.*, 2020, **152**, 124119.
112 The simulations were performed on a regular spatial grid with a spacing of 0.015 Bohr and L = 5.0 Bohr. The dipole impulsive perturbation is $\hat{H}'(t) = -\hat{d}\kappa\delta(t)$, where $\hat{d} = \hat{x}_1 + \hat{x}_2$. After the impulse is applied, the wavefunction is propagated up to 150 Ha^{-1}, employing a time step of 0.002 Ha^{-1}.
113 N. Venkatram, D. N. Rao, L. Giribabu and S. V. Rao, *Appl. Phys. B: Photophys. Laser Chem.*, 2008, **91**, 149–156.
114 T. Takanashi, K. Nakamura, E. Kukk, K. Motomura, H. Fukuzawa, K. Nagaya, S.-i. Wada, Y. Kumagai, D. Iablonskyi, Y. Ito, Y. Sakakibara, D. You, T. Nishiyama, K. Asa, Y. Sato, T. Umemoto, K. Kariyazono, K. Ochiai, M. Kanno, K. Yamazaki, K. Kooser, C. Nicolas, C. Miron, T. Asavei, L. Neagu, M. Schöffler, G. Kastirke, X.-J. Liu, A. Rudenko, S. Owada, T. Katayama, T. Togashi, K. Tono, M. Yabashi, H. Kono and K. Ueda, *Phys. Chem. Chem. Phys.*, 2017, **19**, 19707–19721.
115 M. Mitrano and Y. Wang, *Commun. Phys.*, 2020, **3**, 1–9.
116 B. Buades, A. Picón, E. Berger, I. León, N. Di Palo, S. L. Cousin, C. Cocchi, E. Pellegrin, J. H. Martin, S. Mañas-Valero, E. Coronado, T. Danz, C. Draxl, M. Uemoto, K. Yabana, M. Schultze, S. Wall, M. Zürch and J. Biegert, *Appl. Phys. Rev.*, 2021, **8**, 011408.